21

Thermal Characterization of Solid Structures during Forced Convection Heating

Balázs Illés and Gábor Harsányi
Department of Electronics Technology,
Budapest University of Technology and Economic
Hungary

1. Introduction

By now the forced convection heating became an important part of our every day life. The success could be thanked to the well controllability, the fast response and the efficient heat transfer of this heating technology. We can meet a lot of different types of forced convection heating methods and equipments in the industry (such as convection soldering oven, convection thermal annealing, paint drying, etc.) and also in our household (such as air conditioning systems, convection fryers, hair dryers, etc.).
In every cases the aim of the mentioned applications are to heat or cool some kind of solid materials and structures. If we would like to examine this heating or cooling process with modeling and simulation, first we need to know the physical parameters of the forced convection heating such as the velocity, the pressure and the density space of the flow, together with the temperature distribution and the heat transfer coefficients on the different points of the heated structure. Therefore in this chapter, first we present the mathematical and physical basics of the fluid flow and the convection heating which are needed to the modeling and simulation. We show some models of gas flows trough typical examples in aspect of the heat transfer. We discuss the theory of free-streams, the vertical – radial transformation of gas flows and the radial gas flow layer formation on a plate. The models illustrate how we can study the velocity, pressure and density space in a fluid flow and we also point how these parameters effect on the heat transfer coefficient.
After it new types of measuring instrumentations and methods are presented to characterize the temperature distribution in a fluid flow. Calculation methods are also discussed which can determine the heat transfer coefficients according to the dynamic change of the temperature distribution. The ability of the measurements and calculations will be illustrated with two examples. In the first case we determine the heat transfer coefficient distribution under free gas streams. The change of the heat transfer coefficient is examined when the heated surface shoves out the gas stream. In the second case we study the direction characteristics of the heat transfer coefficient in the case of radial flow layers on a plate in function of the height above the plate. It is also studied how the blocking elements towards the flow direction affects on the formation of the radial flow layer.
In the last part of our chapter we present how the measured and calculated heat transfer coefficients can be applied during the thermal characterization of solid structures. The mathematical and physical description of a 3D thermal model is discussed. The model based

on the thermal (central) node theory and the calculations based on the Finite Difference Method (FDM). We present a new cell partition method, the Adaptive Interpolation and Decimation (AID) which can increase the resolution and the accuracy of the model in the investigated areas without increasing the model complexity. With the collective application of the thermal cell method, the FDM calculations and the AID cell partition, the model description is general and the calculation time of the thermal model is very short compared with the similar Finite Element Method (FEM) models.

2. Basics of convection heating and fluid flow

The phrase of "Convection" means the movement of molecules within fluids (i.e. liquids, gases and rheids). Convection is one of the major modes of heat transfer and mass transfer. Convective heat and mass transfer take place through both diffusion – the random Brownian motion of individual particles in the fluid – and by advection, in which matter or heat is transported by the larger-scale motion of currents in the fluid. In the context of heat and mass transfer, the term "convection" is used to refer to the sum of advective and diffusive transfer (Incropera & De Witt, 1990). There are two major types of heat convection:

1. Heat is carried passively by a fluid motion which would occur anyway without the heating process. This heat transfer process is often termed **forced convection** or occasionally heat advection.
2. Heat itself causes the fluid motion (via expansion and buoyancy force), while at the same time also causing heat to be transported by this bulk motion of the fluid. This process is called **natural convection**, or free convection.

Both forced and natural types of heat convection may occur together (in that case being termed mixed convection). Convective heat transfer can be contrasted with conductive heat transfer, which is the transfer of energy by vibrations at a molecular level through a solid or fluid, and radiative heat transfer, the transfer of energy through electromagnetic waves.

2.1 The convection heating

Convection heating is usually defined as a heat transfer process between a solid structure and a fluid (in the following we will use this type of interpretation). The performance of the convection heating mainly depends on the heat transfer coefficient and can be characterized by the convection heat flow rate from the heater fluid to the heated solid material (Newton's law) (Castell et al., 2008; Gao et al., 2003):

$$\frac{dQ_c}{dt} = F_c = h \cdot A \cdot (T_h(t) - T_t(t)) \qquad [\mathrm{w}] \tag{1}$$

where A is the heated area [m^2], $T_h(t)$ is the temperature of the fluid [K], $T_t(t)$ is the temperature of the solid material [K] and h is the heat transfer coefficient [W/m^{2}K] on the A area.

The heat transfer coefficient can be defined as some kind of "concentrated parameter" which is characterised by the density and the velocity filed of the fluid used for heating, the angle of incidence between the solid structure and the fluid, and finally the roughness of the heated surface (Kays et al., 2004). The value of the heat transfer coefficient can vary between wide ranges but it is typically between 5 and 500 [W/mK] in the case of gases. In a lot of application the material of the fluid and the roughness of the heated surface can be consider

to be constant. Therefore mainly the gas flow parameters (density and velocity) influence the heat transfer coefficient which can be characterized by the mass flow rate q_m (Tamás, 2004):

$$q_m = \int_A \rho \cdot v \cdot dA \qquad [\mathrm{kg/s}] \tag{2}$$

where ρ is the density of the fluid [kg/m^3], v is the velocity of the fluid [m/s] and A is the are whereon q_m is defined.

As you can see in Eq. (1) the calculation of the convection heat transfer is very simple if we know the exact value of the heat transfer coefficient. The problem is that in most of the cases this value is not known. Although we know the influence parameters (velocity, density, etc.) on the heat transfer coefficient but the strength of dependence from the different parameters changes in every cases. There are not existed explicit formulas to determine the heat transfer coefficient only in some special cases.

Inoue (Inoue & Koyanagawa, 2005) has approximated the h parameter of the heater gas streams from the nozzle-matrix blower system with the followings:

$$h = \frac{\lambda}{d} \frac{\sqrt{(\pi/4)(D/l)^2}\left(1 - 2.2\sqrt{(\pi/4)(D/l)^2}\right)}{1 + 0.2(H/D - 6)\sqrt{(\pi/4)(D/l)^2}} \mathrm{Re}^{\frac{2}{3}} \mathrm{Pr}^{0.42} \left[1 + \left(\frac{H/d}{0.6/\sqrt{(\pi/4)(D/l)^2}}\right)^6\right]^{-0.05} \tag{3}$$

where λ is thermal conductivity of the gas [W/m.K], d is the diameter of the nozzles, H is the distance between nozzles and the target [m], r is the distance between the nozzles in the matrix [m], Re is the Reynolds number and Pr is the Prandtl number. The Eq. (3) shown above, has been derived from systematic series of experiments. But unfortunately this method only gives an average value of h and can not deal with the changes of the blower system (contamination, aging, etc.). In addition in many cases it is difficult to determine the exact value of some parameters e.g. the velocity and density of the gas which are needed for Re and Pr numbers.

The same problem occurs in case of other approximations e.g. Dittus–Boelter, Croft–Tebby, Soyars, etc. (a survey of these methods can be seen in (Guptaa et al, 2009)). The simplest way to approximate h is carried out with the linear combination of the velocity and some constants (Blocken et al., 2009), but it gives useful results only in case of big dimensions (e.g. buildings). Other methods calculate h from the mass flow (Bilen et al., 2009; Yin & Zhang, 2008; Dalkilic et al., 2009), but in this case determining the mass flow is also as difficult as determining the velocity.

Therefore in most of the cases the easiest way to determine the heat transfer coefficient is the measuring (see details in Section 4), however it is also important that we can study the effect of the environmental circumstances on the h parameter with gas flow models (see details in Section 3).

2.2. Basics of fluid dynamics

The main issue of this topic is the forced convection when the heat is transported by forced movement of a fluid. Therefore the fluid dynamics are important tools during the study of various forced convection heating methods. During the description of fluid movements, Newton 2nd axiom can be applied, which creates relation between the acting forces on the

fluid particles and the change of the momentum of the fluid particles. Take an elementary fluid particle which moves in the flowing space (Fig. 1.a).

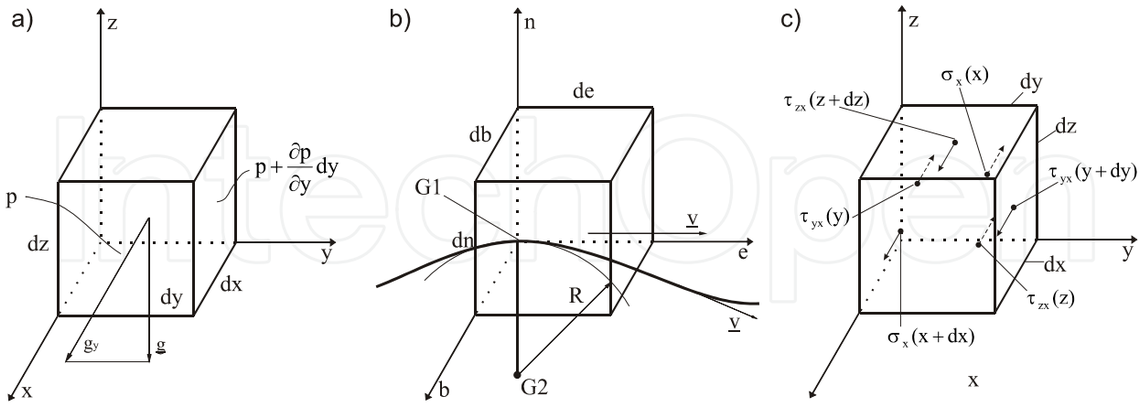

Fig. 1. a) Elementary fluid particle in the flowing phase; b) elementary fluid particle in the flowing phase (natural coordinate system); c) acting stresses towards the *x* direction.

The acting forces are originated from two different sources:

- forces acting on the mass of the fluid particles (e.g. gravity force),
- forces acting on the surface of the fluid particles (e.g. pressure force).

According to these the most common momentum equation – when the friction is neglected and the flow is stationer – is the Euler equation (Tamás, 2004):

$$v\frac{dv}{dr} = g - \frac{1}{\rho}gradp \tag{4}$$

where v is the velocity of the fluid [m/s], t is the time [s], g is the gravity force, ρ is the density [kg/m^3] and p is the pressure. Another important form of this equation – which is often used in the case of the vertical–radial transformation of fluid flows (see in Section 3.) – is defined in natural coordinate system (Fig. 1.b). The natural coordinate system is fixed to the streamline. The connection point is G1. The tangential (e) and the normal (n) coordinate axis are in one plan with the velocity vector (v). In the ambiance of G1 the streamline can be supplemented by an arc which has R radius and G2 center. In this natural coordinate system the Euler equation (vector form) is the following (Tamás, 2004):

$$v\frac{\partial v}{\partial e} = g_e - \frac{1}{\rho}\frac{\partial p}{\partial e} \text{ and } -\frac{v^2}{R} = g_n - \frac{1}{\rho}\frac{\partial p}{\partial n} \text{ and } 0 = g_b - \frac{1}{\rho}\frac{\partial p}{\partial b} \tag{5}$$

In the previous equations we have neglected the effect of friction. However in a lot of convection heating examples this is a non-accurate approach. In the area where the moving fluid touches a solid material the effect of friction can be considerable both form the point of the flowing and the heating. The effect of friction can be determined as some kind of force acting on the surfaces of the moving fluid particle such as the pressure. In Fig. 1.c the stresses acting towards the *x* direction is presented.

The sheer stresses (τ) [Pa] and the tensile stresses (σ) [Pa] usually changes in space and this changes cause the accelerating force on the fluid particle. The stress tensor is:

$$\underline{\underline{\Phi}} = \begin{bmatrix} \sigma_x & \tau_{yx} & \tau_{zx} \\ \tau_{xy} & \sigma_y & \tau_{zy} \\ \tau_{xz} & \tau_{yz} & \sigma_z \end{bmatrix} \tag{6.1}$$

In most of the cases the tensile stresses are caused by only the pressure, therefore:

$$\sigma = -p \tag{6.2}$$

and the sheer stresses can be defined according to the Newton's viscosity law:

$$\tau_{yx} = \mu\left(\frac{\partial v_y}{\partial x} + \frac{\partial v_x}{\partial y}\right) \tag{6.3}$$

where μ is the viscosity of the fluid [kg/m.s]. So τ_{yx} means the tensile stress towards the x direction on the plane with y normal. The other tensile stresses can be defined by the similar way. With the application of the stress tensor the momentum equation can be expressed (the flow is still stationer):

$$v\frac{dv}{dr} = g + \frac{1}{\rho}\underline{\underline{\Phi}}\underline{\nabla} \tag{7}$$

where $\underline{\nabla}$ is the nabla vector. The vector form of the momentum equation is more interesting and more often used which is:

$$v_x\frac{\partial v_x}{\partial x} + v_y\frac{\partial v_x}{\partial y} + v_z\frac{\partial v_x}{\partial z} = g_x + \frac{1}{\rho}\left(-\frac{\partial p}{\partial x} + \mu\left(\frac{\partial^2 v_y}{\partial x^2} + \frac{\partial^2 v_x}{\partial y \partial x}\right) + \mu\left(\frac{\partial^2 v_z}{\partial x^2} + \frac{\partial^2 v_x}{\partial z \partial x}\right)\right) \tag{8.1}$$

$$v_x\frac{\partial v_y}{\partial x} + v_y\frac{\partial v_y}{\partial y} + v_z\frac{\partial v_y}{\partial z} = g_y + \frac{1}{\rho}\left(\mu\left(\frac{\partial^2 v_x}{\partial y^2} + \frac{\partial^2 v_y}{\partial x \partial y}\right) - \frac{\partial p}{\partial y} + +\mu\left(\frac{\partial^2 v_z}{\partial y^2} + \frac{\partial^2 v_y}{\partial z \partial y}\right)\right) \tag{8.2}$$

$$v_x\frac{\partial v_z}{\partial x} + v_y\frac{\partial v_z}{\partial y} + v_z\frac{\partial v_z}{\partial z} = g_z + \frac{1}{\rho}\left(\mu\left(\frac{\partial^2 v_x}{\partial z^2} + \frac{\partial^2 v_z}{\partial x \partial z}\right) + \mu\left(\frac{\partial^2 v_y}{\partial z^2} + \frac{\partial^2 v_z}{\partial y \partial z}\right) - \frac{\partial p}{\partial z}\right) \tag{8.3}$$

3. Application examples of convection heating

In the followings we concentrate only for forced convection heating methods which apply some kind of gas flows. The gas flows can be usually considered to be laminar; therefore the analysis of them is much easier than other fluid flows where this condition is not existed. In this Section typical convection heating applications is studied from the point of gas flow. Simple gas flow models are presented to examine how the changes of the flow parameters effect on the value of the heat transfer coefficient.

The most common and widely used example for the convection heating is the heating with concentrated gas streams. The gas streams blow trough nozzles with d_0 diameter into a free space where the heat structure is placed. Before the deeper analysis, we will discus the basic of this technology which is the free-stream theory.

3.1 Free-stream theory

The free-stream is a single gas stream blown trough a nozzle into the free space (Fig. 2). There are no blocking objects facing to the stream. The free-streams can be studied according to simple and overall rules which are the followings: the initial velocity of the gas is v_0 – instead of the close ambience of the nozzle wall – and the flow is laminar. The out blowing free-stream contacts and interacts with the standing gas in the free space around the circuit of the stream. Therefore the free-stream budges and grips more and more from the standing gas while the radius of the circle where the stream velocity is still v_0 narrows due to the braking effect of the standing gas.

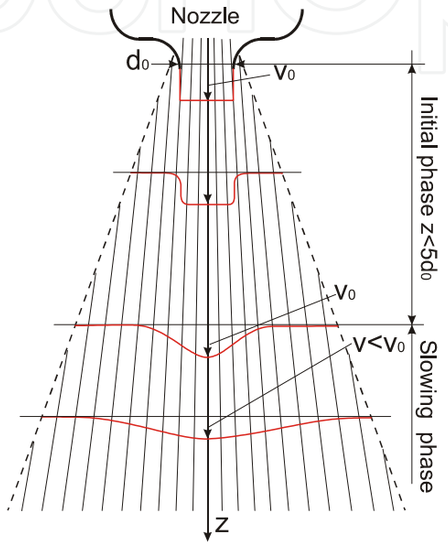

Fig. 2. Cylinder symmetrical free-stream.

The narrowing rate is proportional with distance from the nozzle. Around at $z \cong 5d_0$ distance the velocity of the stream is equal with v_0 only in the axis of the out blowing (Fig. 2). The distance between the out blowing and $z \cong 5d_0$ is the initial phase of the free-stream, if $z > 5d_0$ the stream is in the slowing phase.

The initial value of the heat transfer coefficient is h_0 at the out blowing, and this can be considered to be constant under the nozzle in the initial phase, since the mass flow rate is near constant (Eq. (2)). In the other parts of the stream the heat transfer coefficient increases from the out blowing, but in the initial phase it is smaller than h_0 at least with one order of magnitude. In the slowing phase the mass flow rate decreases exponentially under the nozzle with the heat transfer coefficient, and it is near equalized in the whole free-stream before the gas flow velocity becomes zero.

3.2 Heating with gas streams

Our basic case study is the following: we heat a brick-shape by gas streams from a nozzle-matrix (Fig. 3). We assume that the heated structure is closer to the nozzles than the boarder of the initial phase (defined in Section 3.1). The size of the nozzle-matrix is bigger than the heated structure; around and under the heated structure we defined free space. The nozzle-matrix generates numerous vertical gas streams. We consider the inlet gas streams to be laminar (inlet condition). The diameter of the nozzles are much smaller than the horizontal sizes of heated structure, hence the heated brick-shape effects on the gas streams as a

blocking element. Therefore we model the gas flow on the following criteria which is that the vertical gas streams from the nozzle-matrix turn and join into a continuous radial flow layer (outlet condition) above the brick-shape. At a given point on the surface of the brick-shape the flow direction of the radial layer is determined by a so called "balance line". The balance line marks that location where the main flow direction is changed.

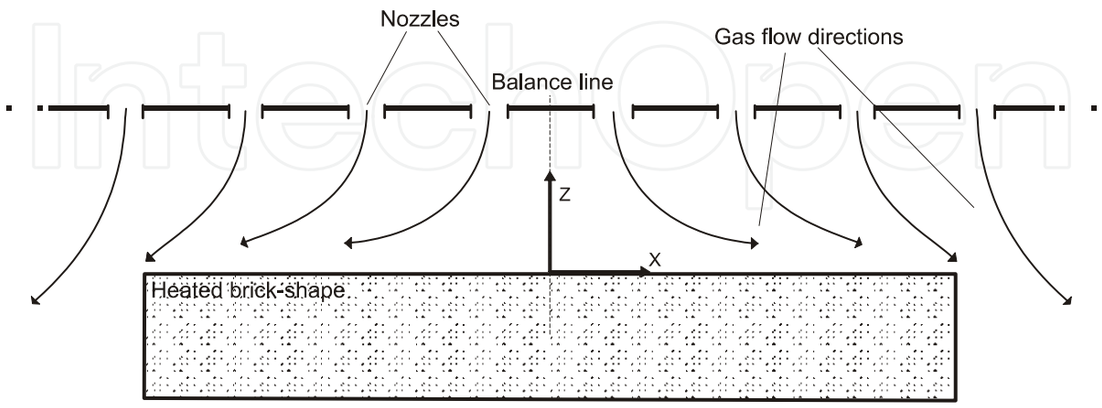

Fig. 3. Gas flows above the heated structure, cross-section, *x* axis.

The schematic view of the gas flow can be seen along the *x* axis in Fig. 3. The zero point of the coordinate system is placed onto the geometrical centre of the heated surface. The direction of a gas stream from a given nozzle depends on the position of the heat structure under the nozzle-matrix. If the system is symmetrical along the *x* axis, this enables us to assume that the transported mass and energy are nearly equal in the $-x$ and $+x$ directions.
However if the system is not symmetric, the balance line is shifted onto asymmetrical position. We have illustrated an example in Fig. 4 where a wall is placed near the heated structure perpendicular to the *y* axis. In this case due to the blocking effect of the wall on the radial flow layer, the transported mass and energy has to be smaller into the –y direction than into the y direction.
Henceforward we study the vertical–radial flow transformation (the radial flow layer formation) of a single gas stream and examine how the transformation effect on the *h* parameter. The model of an inlet vertical gas stream can be seen in Fig. 5. The changes of the flow parameters are much faster than the changes of the gas temperature.

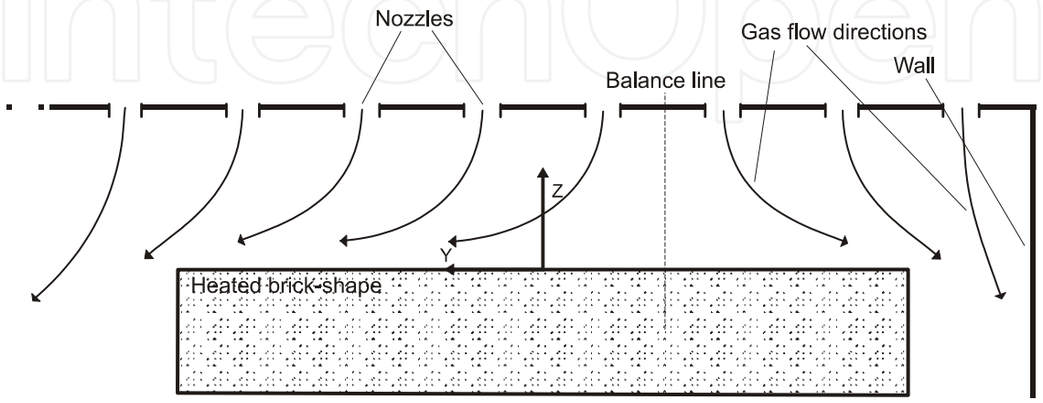

Fig. 4. Gas flows above the heated structure, cross-section, *y* axis.

Therefore the gas flow model of the radial layer formation can be considered as isothermal and stationary. The radial flow layer is separated into further layers from *L(1)* to *L(m)*. In these *L* layers, the velocity of the gas flow, the pressure and the density of the gas are considered to be constant. In Fig. 5 the broken lines represent the borders of *L* flow layers and not streamlines.

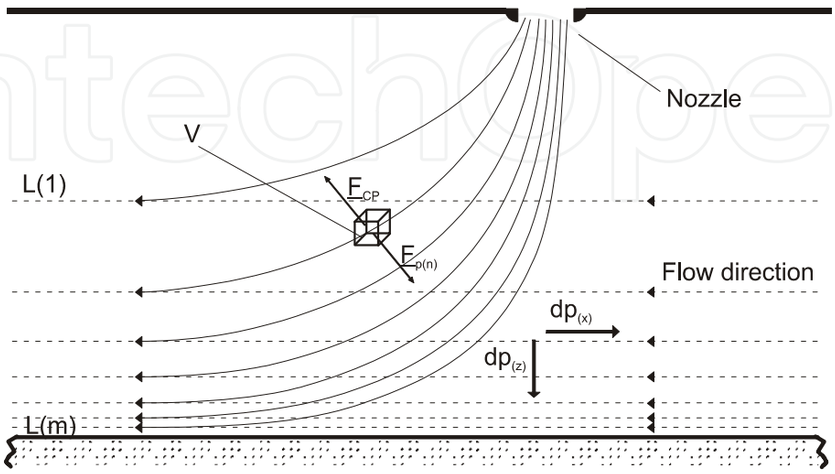

Fig. 5. Radial layer formation, cross-section *x* axis.

We examine the movement of an elemental amount of gas in a constant *V* volume. The m_g mass [kg] in the *V* volume [m³] passes to the radial layer along an arc. During this an F_{CP} centripetal force [N] and an $F_{p(n)}$ force [N] from the pressure change (normal to the movement orbit) acts on the m_g of *V*. The force of the pressure change is defined in a normal coordinate system by the simplified Euler equation (5.2):

$$\underline{F}_{p(n)} = m_g \cdot \frac{|\underline{v}|^2}{R_a} = m_g \cdot \frac{1}{\rho} \cdot \frac{\mathrm{d}p}{\mathrm{d}n} \tag{9}$$

The layer scaling effect of the entrance gas stream starts towards the direction of the radial flow layer. The radiuses of the arcs decrease from *L(1)* to *L(m)*. It occurs that $\mathrm{d}p_n(1) < \mathrm{d}p_n(2) < \ldots < \mathrm{d}p_n(m)$ and the density of the gas also grows towards the heated structure (caused by the isothermal condition).
The momentum equation system in the stationary model is described by Eq. (7):

$$\underline{v} \cdot \frac{\partial \underline{v}}{\partial \underline{r}} = \frac{1}{\rho} \cdot \underline{\underline{\Phi}} \cdot \underline{\nabla} \tag{10}$$

In case of gas flow the gravity force can be neglected. As we defined in Section 2, the $\underline{\underline{\Phi}}$ contains tensile σ [Pa] and shear τ [Pa] stresses. In the gas flow model the tensile stresses are $\sigma_{xx} = \sigma_{yy} = \sigma_{zz} = -p$ and the shear stresses are caused by the friction. Significant friction occurs only between the *L(m)* layer and the surface of the heated structure. Therefore, only

$$\sigma_{zx} = \mu \cdot (\partial v_x / \partial z) \text{ and } \sigma_{zy} = \mu \cdot (\partial v_y / \partial z) \tag{11}$$

have been considered (in both cases the change of the v_z component along the x and y axes can be neglected). So the stress tensor (Eq. (6.1)) can be reduced and this contains only the following elements:

$$\underline{\underline{\Phi}} = \begin{bmatrix} -p & 0 & \mu \cdot (\partial v_x / \partial z) \\ 0 & -p & \mu \cdot (\partial v_y / \partial z) \\ 0 & 0 & -p \end{bmatrix} \tag{12}$$

According to the reduced stress tensor (12) some members of the left side of the momentum Eq. (8) is reduced:

$$v_x \cdot \frac{\partial v_x}{\partial x} + v_z \cdot \frac{\partial v_x}{\partial z} = \frac{1}{\rho} \cdot \left(\mu \cdot \frac{\partial^2 v_x}{\partial z \partial x} - \frac{\partial p}{\partial x} \right) \tag{13.1}$$

$$v_y \cdot \frac{\partial v_y}{\partial y} + v_z \cdot \frac{\partial v_y}{\partial z} = \frac{1}{\rho} \cdot \left(\mu \cdot \frac{\partial^2 v_y}{\partial z \partial y} - \frac{\partial p}{\partial y} \right) \tag{13.2}$$

$$v_z \cdot \frac{\partial v_z}{\partial z} = \frac{1}{\rho} \cdot \left(-\frac{\partial p}{\partial z} \right) \tag{13.3}$$

The equations from (13.1) to (13.3) show that mainly the change of the pressure affects on the velocity. (Except of the *L(m)* layer where the friction is considerable). It was discussed that the pressure in the *L* flow layers increases when getting closer to the heated structure (Fig. 5). This results in that v_z decreases along the z direction towards the brick-shape and causes the decrease of heat transfer coefficient of the inlet gas streams along the z direction when getting closer to the heated structure. Besides the heat transfer coefficient of the radial flow layer has to increase when getting closer to the heated structure while the v_x and v_y velocity components and the density increase. The larger density and velocity should give larger mass flow (according to Eq. (2)) and heat transfer coefficient in the lower radial flow layers.

Consequently the heat transfer coefficients during the vertical-radial flow transformation changes in the following way: the h parameter of the inlet gas streams have to decrease towards the heated structure due to the slew of the velocity vector. Contrarily the h parameter of the radial flow layer has to increase towards the heated structure due to the velocity and density increase.

In the next Section, the effects of the vertical–radial flow transformation and the blocking elements on the heat transfer coefficient are examined and proved by measurements.

4. Measurement methods of the heat transfer coefficient

As we have discussed in Section 2, in most of the cases the only exact solution to determine the heat transfer coefficient is the measurement. Therefore in this section two measurement and calculation methods are presented; with these the h parameter can be determined in the previously discussed cases (Section 3.2).

4.1 Measurement methods

The *h* parameter can be directly calculated form Eq. (1), if we can measure the temperature changes during the convection heating. First we present a method to measure the heat transfer coefficient of the inlet gas streams in function of the height above the heated structure.

The temperature changes have to be measured with the minimum of disturbance to the gas streams. Therefore, point probes have to be used for this purpose. The K-Type rigid (steel coat) thermocouples are suitable with a 1mm diameter. An installation of the measuring can be seen in Fig. 6.

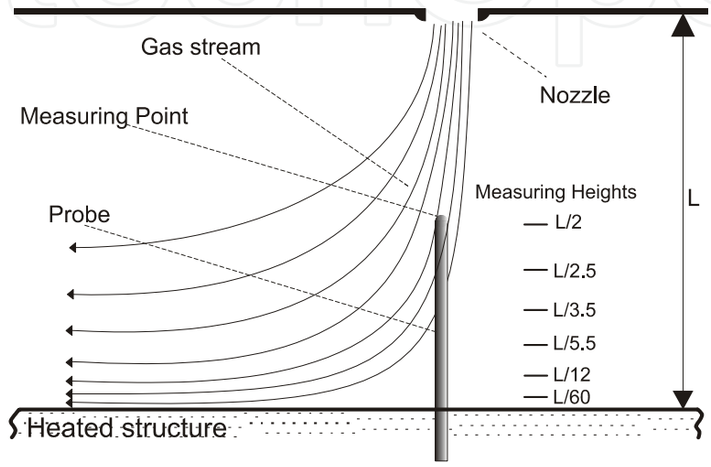

Fig. 6. Measuring installation (inlet gas streams, cross-sectional view).

Their rigid coating has ensured that the thermocouples are being kept in appropriate position during the measurements. The thermo-couple is pinned through a prepared hole of the heated structure. A model structure can be used instead of the real structure; the point is that the shape of the model and the real structure has to be similar. The measurements have to be done below the nozzles facing towards the entrance gas streams.

For the study of the *h* parameter changes of the inlet gas streams above the heated structure, the measurements has to be done at different measurement heights. The measurements have to start at that height where the velocity changes of the inlet gas streams start. The rule of thumb is that this point is near *L/2* (where *L* is the distance between the nozzle-matrix and the heated structure). In our case study we have chosen six measuring heights from the heated structure: *L/60, L/12, L/5.5, L/35, L/2.5* and *L/2* (but these are optional).

If the measurements are repeated at different locations under the nozzle-matrix, the distribution of the heat transfer coefficient can be determined in the function of the height above the heated structure. This kind of distribution measurements can be useful to investigate the inhomogeneity of the heater system (nozzle-matrix).

For the study of the heat transfer coefficient in the radial flow layer, the measurement installation can be seen in Fig. 7.a. The probes are fixed in a measuring gate (measuring box) which held them in position. The front and the rear end of the gate were opened so the radial flow could pass through it, but the roof of the gate protected the probes from the disturbing effect of the inlet gas streams. The probes can be put into the gate through holes on the lateral sides. The gate can be made from any heat insulator material. The size of the gate depends on the diameter of the nozzles and the distance between the nozzle-matrix and

the heated structure. The suitable gate is enough narrow to ensure exact sampling but enough wide to not cause turbulence in the radial flow layer and enough length to protect the probes the from the disturbing effect of the inlet gas streams; optimal width and length is $5...6 \cdot d_{nozzle}$. The height is dedicated by the measurement heights.

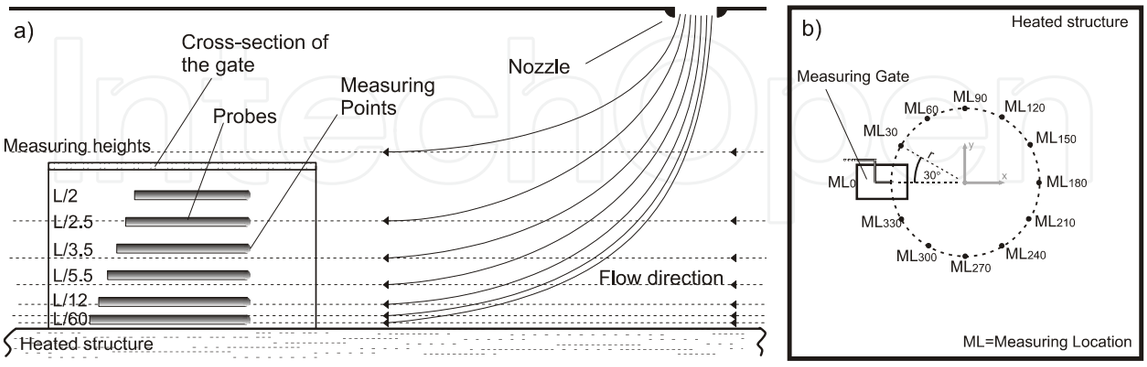

Fig. 7. a) Measuring installation (radial flow layer, cross-sectional view); b) measuring locations (MLs) on the heated structure (upper view).

An advantage of this arrangement was that the probes only obstruct the flow at the measuring points because they were parallel to the radial flow layer. The obstruction and measuring points were overlapped and the disturbance of the radial layer was minimal. During the measurements the same measuring heights are practical to use than in the case of the vertical measurements. With this method the heat transfer coefficient of the radial flow layer can be determined in function of height above the heated structure.

The nature of the radial flow layer can cause that the heat transfer coefficient depends not only on the height but also on the flow direction (as we have seen it in the case of blocking elements, Fig. 4). Therefore the measurements of the h parameter in the radial flow layer have to be done as some kind of direction characteristic measurements. We have to measure the temperature changes at different locations in the radial flow layer. The Measuring Locations (MLs) are located equally around a circle whose centre aligned with the centre of the heated structure (Fig. 7.b). The measuring gate was positioned at the MLs facing towards the centre of the heated structure. The radius of the circle is about the quarter of the smaller plane dimension of the heated structure. For our case study we have chosen 12 MLs.

4.2 Calculation method

The h parameters can be calculated using the heat equation of the investigated thermal system:

$$Q_a = Q_c - Q_k \tag{14}$$

where Q_a is the absorbed thermal energy [J], Q_c is the convection thermal energy [J] and Q_k is a parasite conduction thermal energy [J] caused by measurement system. During the measurements the data logger system is usually colder than the measurement probes; therefore some of the convection heat flows towards the data logger trough the thermo-couples. In most cases of the convection heating the infra-radiation can be neglected.

The measured curves (the temperature changes) showed exponential saturation. Analytical curves have to be fitted to the measured curves for to calculate the *h* parameter. The temperature changes are modeled with exponential saturation:

$$T(t) = (T_h - T(t_0)) \cdot (1 - e^{-t/\tau}) \tag{15.1}$$

where T_h is the heater (gas) temperature, $T(t_0)$ is the initial temperature of the probe, t is the time and τ is the time coefficient of the heating:

$$\tau = t / \ln\left(1 - (T(t_r) - T(t_0)) / (T_h - T(t_0))\right) \tag{15.2}$$

where $T(t_r)$ is the maximum temperature reached at the end of the heating.

Although we know the set temperatures in during the heating, but these are not equal to T_h as in most of the cases the measuring device has a cooling effect on the heater system. This effect depends on the size (thermal capacity) and the temperature differences between the measurement system and the heater gas. In addition the heater system often tries to hold the set temperatures with some kind of temperature control system. Therefore, the exact T_h values of the measured curves are not known, they have to be calculated. This task can be carried out by an iteration curve fitting method.

The T_h is iterated from the value of $T(t_r)$ using a 0.01°C temperature step up. In each iteration steps, the model curves are fitted onto the measured curve. The iteration stops when the fitting failure reaches the minimal value. In Fig. 8, the dashed curve is calculated with only one T_h value (one fitting curve) for the whole curve. But T_h is changing during the measurement. If two T_h values are applied (two fitting curves) – one for the first part [t_0, t_1] and one for the second part [t_1, t_r] of the curve – the matching is much better (continuous line). In other cases more than two T_h values can be also applied in order to reach the best fitting of the analytical curve. Typically in those cases when the heating takes a long time or contrariwise the gradient of the heating is high and the heat capacity of the heated structure is large.

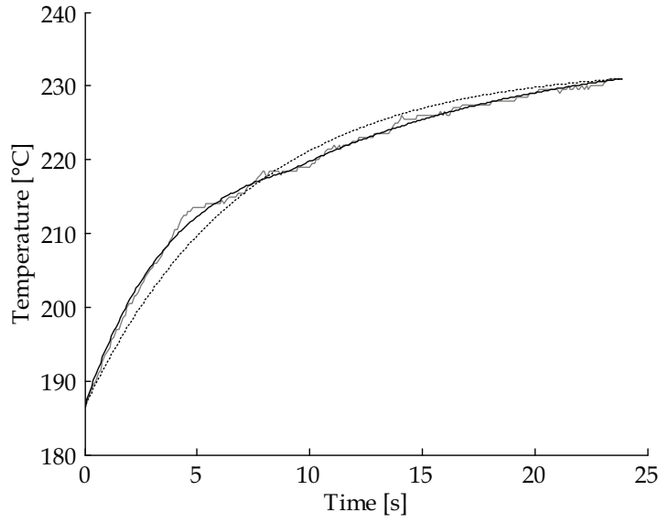

Fig. 8. Analytical curve fitting.

According to the foregoing Eq. (15) has to be modified:

$$T(t) = (T_h(t) - T(t_0)) \cdot (1 - e^{-t/\tau(t)}) \tag{16.1}$$

where

$$T_h(t) = \left[T_{h1}\big|_{0-t_1} ; T_{h2}\big|_{t_1-t_2} ; \ldots ; T_{hn}\big|_{t_{n-1}-t_r} \right] \tag{16.2}$$

and

$$\tau(t) = \left[\tau_1\big|_{0-t_1} ; \tau_2\big|_{t_1-t2} ; \ldots ; \tau_n\big|_{t_{n-1}-tr} \right] \tag{16.3}$$

The convection heat is calculated with the integration of Eq. (1) to the time interval of the heating [t_0, t_r]:

$$Q_c = \int_{t_0}^{t_r} F_c(t)\, dt = \int_{t_0}^{t_r} h \cdot A \cdot (T_h(t) - T(t)) \tag{17}$$

Although the absolute measurement inaccuracy of the thermo-couples is ±0.5°C, but the expected value of the measurement failure is converging to zero due to the integration in Eq. (17).

The thermo couples are well insulated from the steel coat decreasing the conduction impact from the environment. But the parasite conduction resistances of the thermo-couple wires have to be also considered between the data recorder (DR) and the Measuring Point (MP). The conduction model of the measuring system can be seen in Fig. 9, in the case of a K-type thermo-couples which materials are NiCr(90:10) and NiAl(95:5).

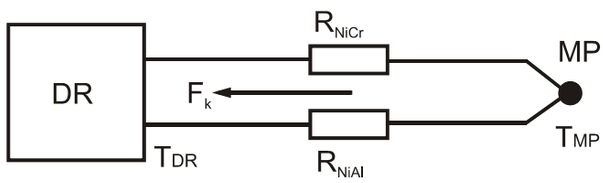

Fig. 9. Conduction model of the measuring system (illustration only for one probe).

The MP is modeled as a sphere and its conduction behavior is neglected because of the small dimensions. The thermal potential difference between the DR and MP generates the parasite conduction heat flow F_k on R_{NiCr} and R_{NiAl}:

$$\frac{dQ_k}{dt} = F_k = \frac{T_{MP} - T_{DR}}{R_{NiCr}} + \frac{T_{MP} - T_{DR}}{R_{NiAl}} \tag{18}$$

The Q_k parasite conduction heat is calculated with the integration of Eq. (18) to the time interval of the heating [t_0, t_r]:

$$Q_k = \int_{t_0}^{t_r} F_k(t) = \int_{t_0}^{t_r} \frac{T(t) - T_{DR}(t)}{R_{NiCr}} + \frac{T(t) - T_{DR}(t)}{R_{NiAl}} \tag{19}$$

The $T_{DR}(t)$ can be approximated with a liner curve which gradient depends on the circumstances of the heating (the temperature change of the data register) during the measurements:

$$T_{DR}(t) = T_0 + (T_0 - T_{DR}(t_r)) \cdot \frac{t}{t_r} \tag{20}$$

where T_0 is the initial temperature of the data register. It is supposed that the thermal capacity of the data register is infinite compared to the thermal capacity of the MP; hence the $T_{DR}(t)$ do not change doe to F_k.
The amount of absorbed thermal energy is calculated (Barbin et al., 2010):

$$Q_a = C \cdot m \cdot (T(t_r) - T(t_0)) \tag{21}$$

where C is the thermal capacity [J/kg.K] and m is the mass [kg] of the measuring point. The value of h is calculated according to Eq. (14), (17) and (21):

$$h = (Q_a + Q_k) / \int_{t_0}^{t_r} A \cdot (T_h(t) - T(t)) \quad [\mathrm{W/m^2K}] \tag{22}$$

4.3 Study of the measured heat transfer coefficients

First we present the results of the characteristics measurements of the h parameter in the case of inlet gas streams above a heated structure (Fig. 6). The applied gas was N_2; the velocity was varied between 4 and 8m/s; the distance between the heated structure and the nozzles was varied between 30 and 70mm. The change of the h parameter is illustrated in function of height (Fig. 10); each point of the characteristics was calculated by 24 measured results.
The h parameter can be considered to be constant from the entrance of the gas streams to *L/2.5*; from *L/2.5* to *L/12* the decline starts and follows a linear shape with 2.9–3.9 W/m²K/mm gradient, at *L/12* there is a cut-off point and the gradient of the decline grows. As it has been expected, the changes of h values are very high in function of the measuring height.

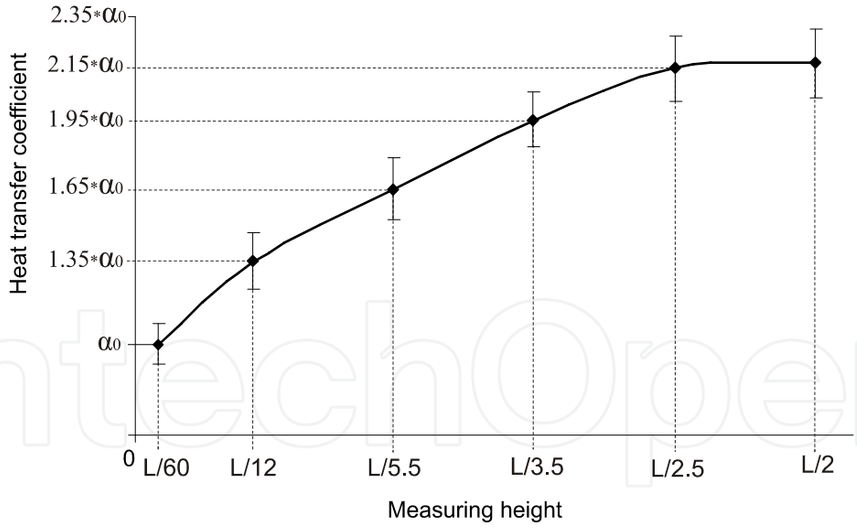

Fig. 10. Characteristics of h parameter of the inlet gas streams in function of height.

These results prove the preconceptions in Section 3.2 that the h parameters of the inlet heater gas streams depend on the height. These are nearly constant (inflowing phase) until a height where the gas flow direction begins to change (transition phase) and the radial layer formation starts. The starting of the transaction begins about at L/2.5 above the heated structure according to the measurements.
As we mentioned in Section 4.1, if the measurements are repeated at different locations under the nozzle-matrix, the distribution of the heat transfer coefficient can be determined

in the function of the height above the heated structure. An example can be seen in Fig. 11 where the efficiency of the nozzle-lines can be compared in a reflow oven at *L/2.5* measuring height (Illés, 2010). This visualization method ensures that we get sufficient view of the changes of *h* parameter in the oven.
The 15–25 % *h* parameter differences were observed between the nozzle-lines. The examined oven is six year old; therefore the differences are probably caused by the inhomogeneity of the gas circulation system (the different attrition of the fans).

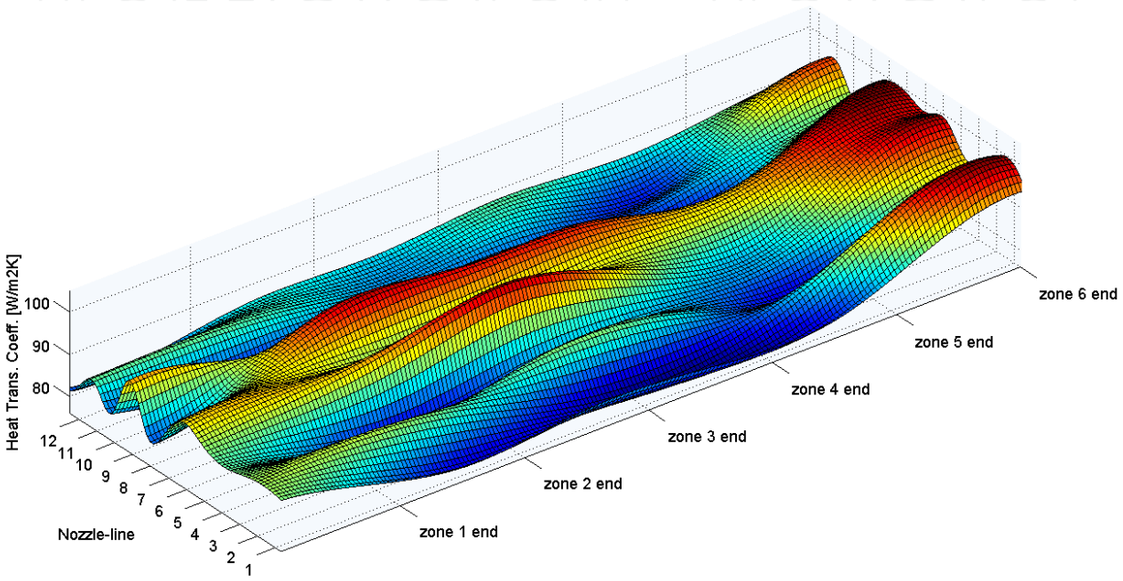

Fig. 11. Distribution of the *h* parameter in the oven at *L/2.5* measuring height.

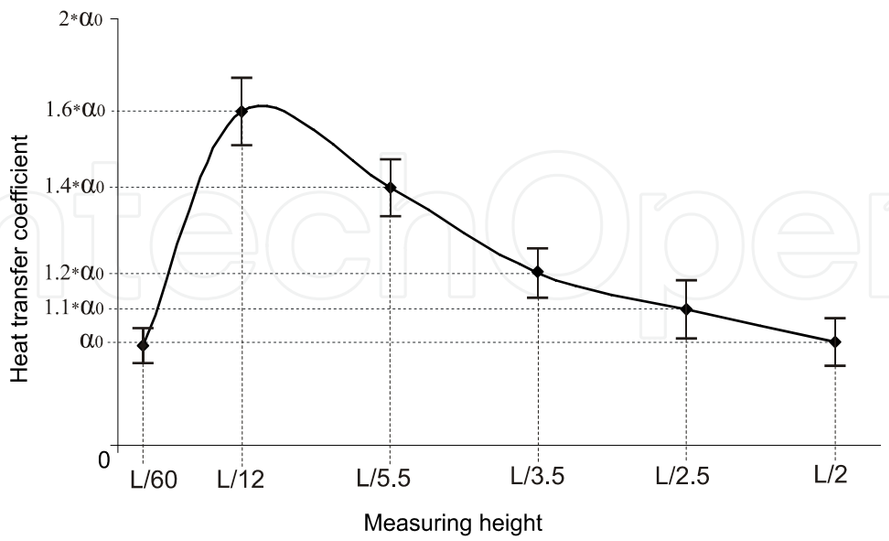

Fig. 12. Characteristics of the *h* parameter in the radial flow layer in function of height.

In Fig. 12 the results of the characteristics measurements of the *h* parameter in the radial flow layer is presented above a heated structure (Fig. 7). The gas flow parameters were the same as

the inlet gas stream measurements. The change of the *h* parameter is illustrated in function of height (Fig. 12); each point of the characteristics was calculated by 24 measured results.
The value of *h* also depends on the measuring height in the radial flow layer. This increases when getting closer to the heated structure until a given distance (peak value is near L/12 distance from the heated structure). This effect is caused by the growth of density and flow rate in the radial layer towards the heated structure, as it was discussed in Section 3.2. However, the friction becomes considerably higher at the closest ambience of the heated structure (L/60). This slows the flow rate (Illés & Harsányi, 2009; Wang et al., 2006; Cheng et al., 2008) more than the growth of the density, and this effect decreases the *h* parameter dramatically. It should be noted that the *h* parameter is near equal at the L/60 and L/2 distances.
As it was discussed in Section 4.1 we can do direction characteristics measurement in the radial flow layer. The *h* values measured at ML_0 – ML_{330} can be presented as 3D directional characteristics of the heat transfer coefficient. This means that we illustrate the *h* values above the *x*-*y* plane according to the MLs and the measuring height. The appropriate values are attached because of the better visualization: the values of a given measuring height are attached with a horizontal curve and the values of a given ML are attached with a vertical curve. In this form, our results are more expressive because the heating capability is analyzable in each direction.

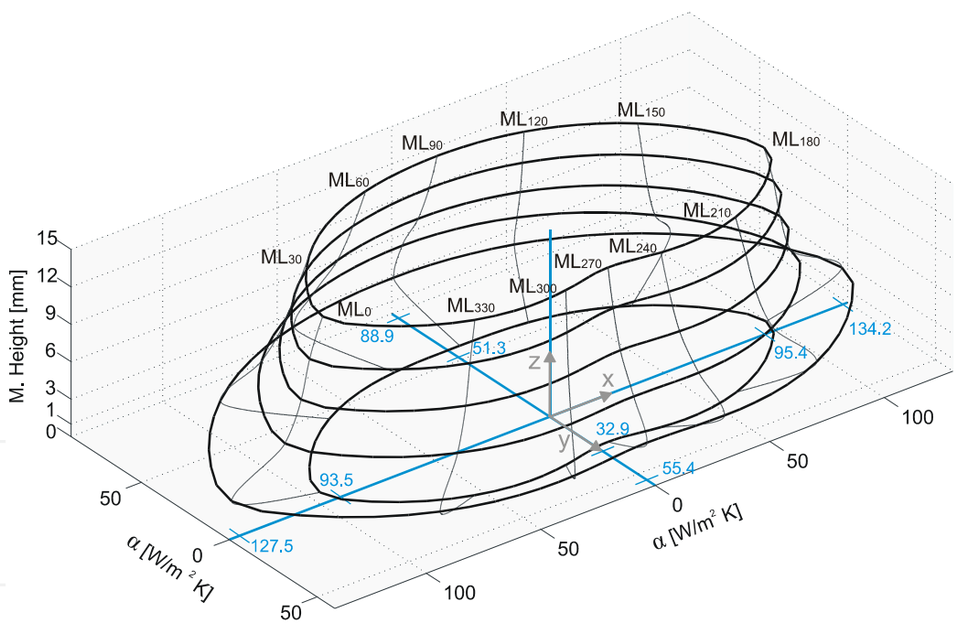

Fig. 13. 3D directional characteristics of the *h* parameter in a convection reflow oven.

In Fig. 13, we show an example to application of the 3D directional characteristics. This present the *h* parameter in the radial flow layer of a convection reflow oven (Illés & Harsányi, 2009). On the main axes (*x* and *y*), the minimum and maximum values of *h* are also marked.
Major heating capability differences can be observed between the directions which are caused by the construction of the oven. We can study the effect of blocking elements (such as walls; Fig. 4 in Section 4.1) on the heat transfer coefficient towards the different directions. The *h* parameters are much larger (80–120%) towards the directions where are no blocking oven walls, than those where these are. In addition, there are also considerable heating

capability differences (30–40%) between the directions towards the opposite oven walls (ML_{90} and ML_{270}). This is caused by the asymmetrical design of the oven (the right wall is closer to the heated structure than the left wall).

5. Modeling the heating of solid structures

In the previous sections we have discussed how the convection heat transfers to the solid structures, how the gas flow circumstances form during the convection heating and how the heat transfer coefficient can be measured. In this section, we present a 3D combined heat transfer and conduction model which can calculate the temperature distribution of the solid structure during the convection heating process. In addition we also show how the measured heat transfer coefficients can be used during the modelling.

5.1 Basics of the heating model

The model is based on the thermal or central node theory. This means that the investigated area is divided into thermal cells representing the thermal behaviour of the given material. We have defined the basic thermal cell as a cuboid (Fig 14.a). This shape is easy to handle and useful for our nonuniform grid.

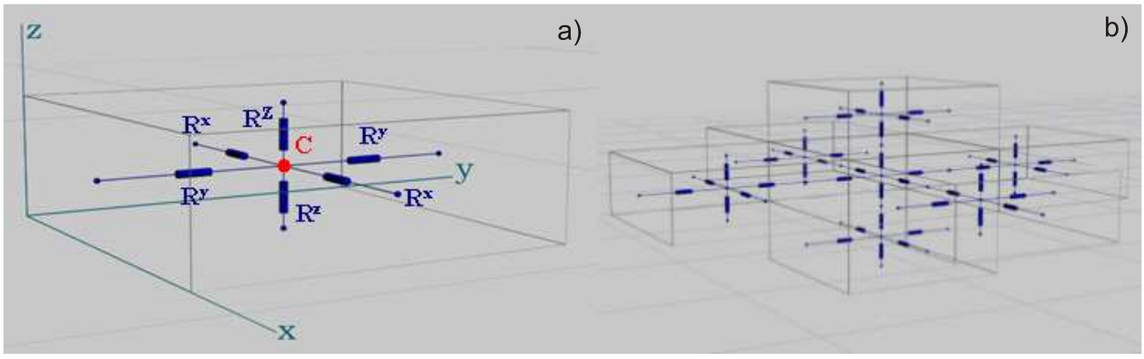

Fig. 14. a) The basic thermal cell; b) neighboring thermal cells.

All cells contain a thermal node in their geometrical centre, which represents the thermal mass of the cell as a heat capacity [J/K]:

$$C = C_S \cdot \rho \cdot V \tag{23}$$

where C_S is the specific heat capacity of the material [J/kg.K], ρ is the density of the material [kg/m^3] and V is the volume of the cell [m^3]. The thermal conduction ability of the cells is described with thermal resistances [K/W] between the node and its cell borders:

$$R^x = \frac{l_x}{2 \cdot \lambda \cdot l_y \cdot l_z} \text{ and } R^y = \frac{l_y}{2 \cdot \lambda \cdot l_x \cdot l_z} \text{ and } R^z = \frac{l_z}{2 \cdot \lambda \cdot l_x \cdot l_y} \tag{24}$$

where l_x, l_y and l_z are the dimensions of the cell [m] and λ is the specific thermal conductivity of the material [W/m.K]. The neighbouring thermal cells are in connections with the thermal resistances (Fig. 14.b).

In most of the cases the application of a non-uniform grid is the most effective; with this the resolution of the model can be refined to focus on areas of interest whilst reducing the involvement with the less important areas. The cell partition method is presented on the

example can be seen in Fig. 15.a which is a surface mounted component on a printed wiring board (Illés & Harsányi, 2008). First we have to choose the object area of the model; in our example this is only the component and its direct environment (marked by red lines around the component).

The construction of the nonuniform grid is very important due to the implementation of the model. We use a simple but very useful condition for the faces of the thermal cells in the nonuniform grid: all neighbouring faces should have the same size. It ensures that all thermal cells can be in direct connection with maximum 6 other cells (all cells can have maximum 6 neighbours). In this case, all the neighbours are known, so the model can be implemented according to the indexing of the cells. Otherwise, (if the number of the neighbours is not maximized) the direct connections between the cells would be fund by mathematical induction, so the implementation of the model would be more complicated.

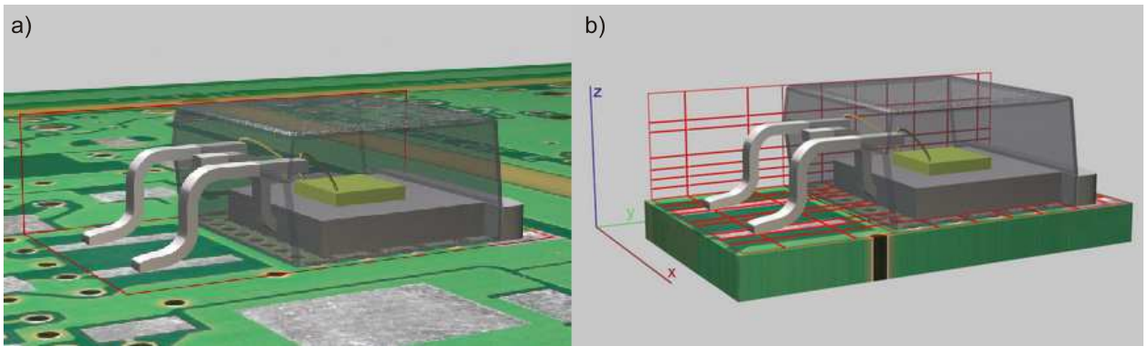

Fig. 15. a) Choose the objective area of the model; b) the nonuniform resolution.

This construction of the nonuniform grid can be achieved by the following steps: we define a basic uniform grid with section planes. The cell borders are the section lines of these planes. After this, adaptive interpolation (in the areas of interest) and decimation (in the less important areas) is done on the section planes separately along each axis. If the degrees of the interpolation and the decimation are the same then the number of cells will not change. A nonuniform grid can be seen in Fig. 15.b. In order to help a better visualization of this concept only some section lines of the section planes are visible in the picture.

According to the thermal node theory there should be thermodynamic equilibrium in all cells. Therefore during the cell partition, the borders of the different materials have to be taken into consideration.

The nonuniform grid gives as more information from the important parts than the uniform with the same cell number. This approach therefore allows to achieve a significant increase of spatial resolution of the calculated temperature distribution in some distinct areas with only a little increase of model complexity.

The cell type and the physical position of the cells can be assigned by the coordinates of the intersections. The indexing of the cells is carried out by numbering the section planes (n_x, n_y and n_z according to the axis). All cells and their cell parameters can then be identified with these numbers: the heat capacity $C(n_x, n_y, n_z)$; the thermal resistances $R^x(n_x, n_y, n_z)$, $R^y(n_x, n_y, n_z)$ and $R^z(n_x, n_y, n_z)$ which also contain the direction of the resistance (Fig. 14.a).

5.2 Model description

The model is described by common heat conduction and convection equations and these are solved by the finite difference method in order to achieve high calculation speed and easy

implementation. If the time steps are small enough then the boundary conditions and material properties can be assumed to remain constant over the time steps. The temperature change in the cells can be calculated by the backward Euler formula:

$$\frac{\mathrm{d}T_n(t)}{\mathrm{d}t} = \frac{T_n(t) - T_n(t-\mathrm{d}t)}{\mathrm{d}t} = \frac{F}{C} \tag{25}$$

where T_n is the temperature of the cell [K], t is the time [s], dt is the time step [s], F is the heat flow rate [W] and C is the heat capacity of the cell [J/K].

We use the following boundary conditions: there is only convection heat change between the solid-gas boundaries, and the convection heat always flows from the gas to the solid (the gas is always hotter than the solid). The solid-solid boundaries of the model (if we study only a part of a solid structure) are considered to be adiabatic. The heat spreads by conduction heat transport between the thermal cells in the model. As formerly, we neglect the radiation heat.

The equation of the convective heat flow rate (Eq. (1)) is used in the following form:

$$F_C(t,\underline{r}) = A_n \cdot h(\underline{r}) \cdot (T_h(\underline{r}) - T_n(t)) \tag{26}$$

where $h(\underline{r})$ is the heat transfer coefficient [W/m²K] depending on the location, A_n is the heated surface [m²] and $T_h(\underline{r})$ is the heater gas temperature [K] depending on the location. The conduction heat flow is caused by the temperature difference between the cells:

$$F_K(t) = \frac{T_{n-1}(t) - T_n(t)}{R_{n-1} + R_n} \tag{27}$$

where R_{n-1} and R_n are the thermal resistances between the adjacent cells, whilst $T_{n-1}(t)$ and $T_n(t)$ are the temperatures of the adjacent cells.

We assume the following initial condition $T_1(0) \cong T_2(0) \cong \ldots \cong T_n(0)$ meaning that, before the heating, the temperature gradient of our system is very small. This assumption is always valid for equilibrium thermodynamics systems. Therefore, between the adjacent cells $F_K(0) \cong 0$, this means that the conduction heat is generated only by convection heating. Using Eq. (25), (26) and (27), this is the general form of the differential equation which describes the temperature change of the cells in the model:

$$\frac{\mathrm{d}T}{\mathrm{d}t} = \frac{1}{C} \cdot \left[\sum_{i=0}^{k} F_{C(i)} + \sum_{j=1}^{6-k} F_{K(j)} \right] \tag{28}$$

where k is the number of the solid-gas interfaces and 6-k is the number of adjacent cells.

For the description of the whole model, a differential equation system is needed. With an appropriate selection of the cells parameters and initial assumptions, the differential equation system can be easily generated. The indexing method, shown in Section 5.1, will be our starting point. All cells have an own heat capacity, six faces and six thermal resistances from the six faces. The heat capacities can be handled as values $C(n_x, n_y, n_z)$, the surfaces and thermal resistances are stored in vectors and matrixes.

Although all cells have only three different surfaces, these are stored in 6x6 element matrixes, it will be useful for general implementation:

$$\underline{\underline{A}}(n_x,n_y,n_z)=\begin{bmatrix} A^x(n_x,n_y,n_z) & 0 & 0 & 0 & 0 & 0 \\ 0 & A^{-x}(n_x,n_y,n_z) & 0 & 0 & 0 & 0 \\ 0 & 0 & A^y(...) & 0 & 0 & 0 \\ 0 & 0 & 0 & A^{-y}(...) & 0 & 0 \\ 0 & 0 & 0 & 0 & A^z(...) & 0 \\ 0 & 0 & 0 & 0 & 0 & A^{-z}(...) \end{bmatrix} \tag{29}$$

where $A^x(n_x,n_y,n_z)=A^{-x}(n_x,n_y,n_z)$, these are opposite faces of the cell which are perpendicular to x axis, etc. For the general implementation the thermal resistances should be transformed to thermal conductances. The $\underline{G}(n_x,n_y,n_z)$ vectors have the following form:

$$\underline{G}(n_x,n_y,n_z)=\begin{bmatrix} G^x(n_x,n_y,n_z)\cdot G^x(n_x-1,n_y,n_z)/(G^x(n_x,n_y,n_z)+G^x(n_x-1,n_y,n_z)) \\ G^x(n_x,n_y,n_z)\cdot G^x(n_x+1,n_y,n_z)/(G^x(n_x,n_y,n_z)+G^x(n_x+1,n_y,n_z)) \\ G^y(n_x,n_y,n_z)\cdot G^y(n_x,n_y-1,n_z)/(G^y(n_x,n_y,n_z)+G^y(n_x,n_y-1,n_z)) \\ G^y(n_x,n_y,n_z)\cdot G^y(n_x,n_y+1,n_z)/(G^y(n_x,n_y,n_z)+G^y(n_x,n_y+1,n_z)) \\ G^z(n_x,n_y,n_z)\cdot G^z(n_x,n_y,n_z-1)/(G^z(n_x,n_y,n_z)+G^z(n_x,n_y,n_z-1)) \\ G^z(n_x,n_y,n_z)\cdot G^z(n_x,n_y,n_z+1)/(G^z(n_x,n_y,n_z)+G^z(n_x,n_y,n_z+1)) \end{bmatrix} \tag{30}$$

According to the construction of the model, multiplying by zero is carried out in the positions of solid-gas interfaces. These elements of $\underline{G}(n_x,n_y,n_z)$ are zero.
As we have proved in Section 4, the efficiency of the convection heating could be changed on the different faces of the heated structure. We apply the flowing assistant vectors:

$$\underline{h}(n_x,n_y,n_z)=\begin{bmatrix} h^x(n_x,n_y,n_z) \\ h^{-x}(n_x,n_y,n_z) \\ h^y(n_x,n_y,n_z) \\ h^{-y}(n_x,n_y,n_z) \\ h^z(n_x,n_y,n_z) \\ h^{-z}(n_x,n_y,n_z) \end{bmatrix} \tag{31}$$

where $h^x(n_x,n_y,n_z)$ is the heat transfer coefficient on $A^x(n_x,n_y,n_z)$ and $h^{-x}(n_x,n_y,n_z)$ is the heat transfer coefficient on $A^{-x}(n_x,n_y,n_z)$, etc. The elements of $\underline{h}(n_x,n_y,n_z)$ have to be zero at those positions where $\underline{G}(n_x,n_y,n_z)$ are not zero. This means that $\underline{h}(n_x,n_y,n_z)$ are zero on those positions where adjacent cells are located near the given cell.
The temperature differences between the heater gas and the heated cells are also stored in assistant vectors:

$$\underline{T_h}(n_x,n_y,n_z)=\begin{bmatrix} T_h^{\,x}(n_x,n_y,n_z)-T(n_x,n_y,n_z) \\ T_h^{\,-x}(n_x,n_y,n_z)-T(n_x,n_y,n_z) \\ T_h^{\,y}(n_x,n_y,n_z)-T(n_x,n_y,n_z) \\ T_h^{\,-y}(n_x,n_y,n_z)-T(n_x,n_y,n_z) \\ T_h^{\,z}(n_x,n_y,n_z)-T(n_x,n_y,n_z) \\ T_h^{\,-z}(n_x,n_y,n_z)-T(n_x,n_y,n_z) \end{bmatrix} \tag{32}$$

where $T_h^{\,x}(n_x,n_y,n_z)$ is the heater gas temperature at $A^x(n_x,n_y,n_z)$, etc. To achieve a compact description, the temperature differences between a given cell and its adjacent cells are also collected into assistant vectors:

$$\underline{T_K}(n_x,n_y,n_z)=\begin{bmatrix} T(n_x-1,n_y,n_z)-T(n_x,n_y,n_z) \\ T(n_x+1,n_y,n_z)-T(n_x,n_y,n_z) \\ T(n_x,n_y-1,n_z)-T(n_x,n_y,n_z) \\ T(n_x,n_y+1,n_z)-T(n_x,n_y,n_z) \\ T(n_x,n_y,n_z-1)-T(n_x,n_y,n_z) \\ T(n_x,n_y,n_z+1)-T(n_x,n_y,n_z) \end{bmatrix} \tag{33}$$

We need only those values of $\underline{T_K}(n_x,n_y,n_z)$ where adjacent cells exist. Therefore $\underline{T_K}(n_x,n_y,n_z)$ vectors will be filtered by the $\underline{G}(n_x,n_y,n_z)$ vectors. In those positions where the $\underline{G}(n_x,n_y,n_z)$ vector is zero, the value of the $\underline{T_K}(n_x,n_y,n_z)$ will be disregarded. The solid-gas interfaces are chosen by $\underline{h}(n_x,n_y,n_z)$. By the application of the assistant vectors and matrixes (29–33) this gives us the general expression of the differential equation system which best describes the model:

$$\frac{\mathrm{d}T(n_x,n_y,n_z)}{\mathrm{d}t}=\frac{\underline{h}(n_x,n_y,n_z)^T\cdot\underline{\underline{A}}(n_x,n_y,n_z)\cdot\underline{T_h}(n_x,n_y,n_z)+\underline{G}(n_x,n_y,n_z)^T\cdot\underline{\underline{T_K}}(n_x,n_y,n_z)}{C(n_x,n_y,n_z)} \tag{34}$$

If we do not maximize the number of the cell neighbours in the model then the assistant vectors (29), (30), (31) and (33) would be matrices with *6xN* dimensions (*N* is the cell number), therefore Eq. (34) and its implementation would be more complex.

5.3 Application example

In the last section we present an application of our model which is the convectional heating of a surface mounted component (e.g. during the reflow soldering) in Fig 15. We investigate how change the temperature of the soldering surfaces of the component if the heat transfer coefficients are different around the component (see more details in (Illés & Harsányi, 2008)). The model was implemented using MATLAB 7.0 software.

We have defined a nonuniform grid with 792 thermal cells (the applied resolution is the same as in Fig 15.b), the *x-y* projection in the contact surfaces can be seen in (Fig. 16.a). In this grid, the 13 contact surfaces are described by 31 thermal cells. But the cells which represent the same contact surface can be dealt with as one. The examined cell groups are shown as squares in Fig. 16.a.

We use the following theoretical parameters: $T(0)$=175°C; T_h=225°C; h^x=40W/m.K; h^{-x}=75W/m.K; h^y= h^{-y}=100W/m.K; h^z= h^{-z}=80W/m.K. We investigate an unbalanced heating case when there is considerable heat transfer coefficient deviation between right and left faces of the component (Fig. 16.a). The applied time step was dt=10ms. In Fig. 16.b the temperature of the different contact surfaces can be seen at different times.

After 3 seconds from the starts of the heating there are visible temperature difference between the investigated thermal cells occurred by their positions (directly or non-directly heated cells) and different heat conduction abilities. The temperature of the cell groups which are heated directly (1a, 1b, 2a, 2b and 3a–3c) by the convection rises faster than the temperature of the cell groups which are located under the component (4a–4f) and the heat penetrates into them only by conduction way. This temperature differences increase during the heating until the saturation point where the temperature begins to equalize. The effect of the unbalanced heating along the x direction ($h^x \neq h^{-x}$) can also be studied in Fig. 16.b. The cell groups under the left side of the component (1a, 2a, 3a, 4a, 4c and 4e) are heated faster compared to their cell group pair (1b, 2b, 3c, 4b, 4d and 4f) from the left side.

This kind of investigations are important in the case of soldering technologies because the heating deviation results in a time difference between the starting of the melting process on different parts of the soldering surfaces. This breaks the balance of the wetting force which results in that the component will displace during the soldering. According to the industrial results, if the time difference between the starting of the melting on the different contact surfaces is larger than 0.2s the displacement of the component can occur (Warwick, 2002; Kang et al., 2005).

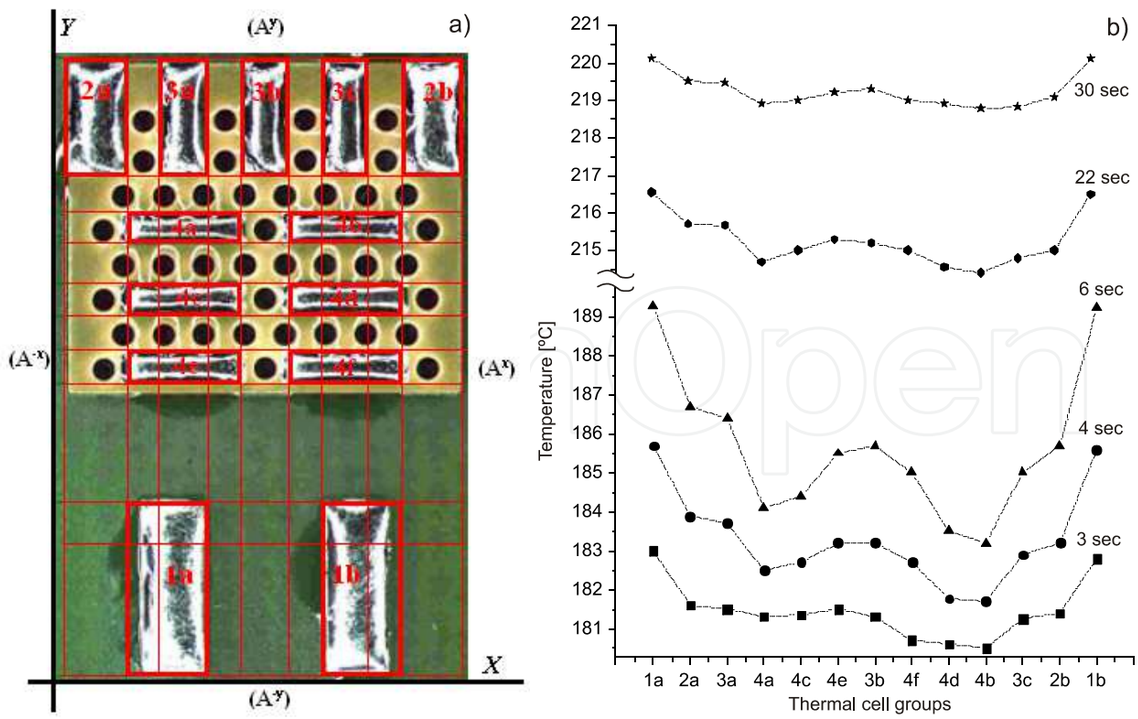

Fig. 16. a) x–y projection of the applied nonuniform grid; b) temperature distribution of the contact surfaces

Comparing the abilities of our model with a general purpose FEM system gave us the following results. The data entry and the generation of the model took nearly the same time in both systems, but the calculation in our model was much faster than in the general purpose FEM analyzer. Tested on the same hardware configuration, the calculation time was less than 3s using our model, while in the FEM analyzer it took more than 52s.

6. Summary and conclusions

In this chapter we presented the mathematical and physical basics of fluid flow and convection heating. We examined some models of gas flows trough typical examples in aspect of the heat transfer. The models and the examples illustrated how the velocity, pressure and density space in a fluid flow effect on the heat transfer coefficient. New types of measuring instrumentations and methods were presented to characterize the temperature distribution in a fluid flow in order to determine the heat transfer coefficients from the dynamic change of the temperature distribution. The ability of the measurements and calculations were illustrated with examples such as measuring the heat transfer coefficient distribution and direction characteristics in the case of free streams and radial flow layers.
We presented how the measured and calculated heat transfer coefficients can be applied during the thermal characterization of solid structures. We showed that a relatively simple method as the thermal node theory can be a useful tool for investigating complex heating problems. Using adaptive interpolation and decimation our model can improve the accuracy of the interested areas without increasing their complexity. However, the time taken for calculation by our model is very short (only some seconds) when compared with the general FEM analyzers. Although we showed results only from one investigation, the modelling approach suggested in this chapter, is also applicable for simulation and optimization in other thermal processes. For example, where the inhomogeneous convection heating or conduction properties can cause problems.

7. Acknowledgement

This work is connected to the scientific program of the " Development of quality-oriented and harmonized R+D+I strategy and functional model at BME" project. This project is supported by the New Hungary Development Plan (Project ID: TÁMOP-4.2.1/B-09/1/KMR-2010-0002).
The authors would like to acknowledge to the employees of department TEF2 of Robert Bosch Elektronika Kft. (Hungary/Hat- van) for all inspiration and assistance.

8. Reference

Barbin, D.F., Neves Filho, L.C., Silveira Júnior, V., (2010) Convective heat transfer coefficients evaluation for a portable forced air tunnel, Applied Thermal Engineering 30 (2010) 229–233.

Bilen, K., Cetin, M., Gul, H., Balta, T., (2009) The investigation of groove geometry effect on heat transfer for internally grooved tubes, Applied Thermal Engineering 29 (2009) 753–761.

Blocken, B., Defraeye, T., Derome, D., Carmeliet, J., (2009) High-resolution CFD simulations for forced convective heat transfer coefficients at the facade of a low-rise building, Building and Environment 44 (2009) 2396–2412.

Castell, A., Solé, C., Medrano, M., Roca, J., Cabeza, L.F., García, D. (2008) Natural convection heat transfer coefficients in phase change material (PCM) modules with external vertical fins, Applied Thermal Engineering 28 (2008) 1676–1686.

Cheng, Y.P., Lee, T.S., Low, H.T., (2008) Numerical simulation of conjugate heat transfer in electronic cooling and analysis based on field synergy principle, Applied Thermal Engineering 28 (2008) 1826–1833.

Dalkilic, A.S., Yildiz, S., Wongwises, S., (2009) Experimental investigation of convective heat transfer coefficient during downward laminar flow condensation of R134a in a vertical smooth tube, International Journal of Heat and Mass Transfer 52 (2009) 142–150.

Gao, Y., Tse, S., Mak, H., (2003) An active coolant cooling system for applications in surface grinding, Applied Thermal Engineering 23 (2003) 523–537.

Guptaa, P.K., Kusha, P.K., Tiwarib, A., (2009) Experimental research on heat transfer coefficients for cryogenic cross-counter-flow coiled finned-tube heat exchangers, International Journal of Refrigeration 32 (2009) 960–972.

Illés, B., Harsányi, G., (2008) 3D Thermal Model to Investigate Component Displacement Phenomenon during Reflow Soldering, Microelectronics Reliability 48 (2008) 1062–1068.

Illés, B., Harsányi, G., (2009) Investigating direction characteristics of the heat transfer coefficient in forced convection reflow oven, Experimental Thermal and Fluid Science 33 (2009) 642–650.

Illés, B., (2010) Measuring heat transfer coefficient in convection reflow ovens, Measurement 43 (2010) 1134–1141.

Incropera, F.P., De Witt, D.P. (1990) Fundamentals of Heat and Mass Transfer (3rd ed.). John Wiley & Sons.

Inoue, M., Koyanagawa, T., (2005) Thermal Simulation for Predicting Substrate Temperature during Reflow Soldering Process, IEEE Proceedings of 55th Electronic Components and Technology Conference, Lake Buena Vista, Florida, 2005, pp.1021-1026.

Kang, S.C., Kim C., Muncy J., Baldwin D.F., (2005) Experimental Wetting Dynamics Study of Eutectic and Lead-Free Solders With Various Fluxes, Isothermal Conditions, and Bond Pad Metallization. IEEE Transactions on Advanced Packaging 2005; 28 (3):465–74.

Kays, W., Crawford, M., Weigand, B., (2004) Convective Heat and Mass Transfer, (4th Ed.), McGraw-Hill Professional.

Tamás, L., (2004) Basics of fluid dynamics, (1st ed.), Műegyetemi Kiadó, Budapest.

Wang, J.R., Min, J.C., Song, Y.Z., (2006) Forced convective cooling of a high-power solid-state laser slab, Applied Thermal Engineering 26 (2006) 549–558.

Warwick, M., (2002) Tombstoning Reduction VIA Advantages of Phased-reflow Solder. SMT Journal 2002; (10):24–6.

Yin, Y., Zhang, X., (2008) A new method for determining coupled heat and mass transfer coefficients between air and liquid desiccant, International Journal of Heat and Mass Transfer 51 (2008) 3287–3297.

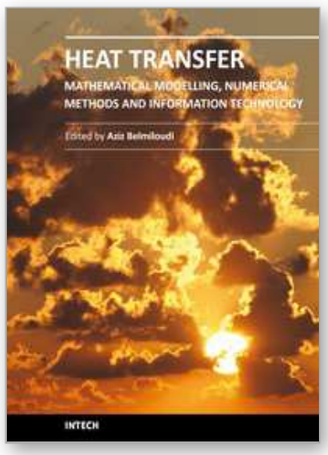

Heat Transfer - Mathematical Modelling, Numerical Methods and Information Technology

Edited by Prof. Aziz Belmiloudi

ISBN 978-953-307-550-1
Hard cover, 642 pages
Publisher InTech
Published online 14, February, 2011
Published in print edition February, 2011

Over the past few decades there has been a prolific increase in research and development in area of heat transfer, heat exchangers and their associated technologies. This book is a collection of current research in the above mentioned areas and describes modelling, numerical methods, simulation and information technology with modern ideas and methods to analyse and enhance heat transfer for single and multiphase systems. The topics considered include various basic concepts of heat transfer, the fundamental modes of heat transfer (namely conduction, convection and radiation), thermophysical properties, computational methodologies, control, stabilization and optimization problems, condensation, boiling and freezing, with many real-world problems and important modern applications. The book is divided in four sections : "Inverse, Stabilization and Optimization Problems", "Numerical Methods and Calculations", "Heat Transfer in Mini/Micro Systems", "Energy Transfer and Solid Materials", and each section discusses various issues, methods and applications in accordance with the subjects. The combination of fundamental approach with many important practical applications of current interest will make this book of interest to researchers, scientists, engineers and graduate students in many disciplines, who make use of mathematical modelling, inverse problems, implementation of recently developed numerical methods in this multidisciplinary field as well as to experimental and theoretical researchers in the field of heat and mass transfer.

InTech Europe
University Campus STeP Ri
Slavka Krautzeka 83/A
51000 Rijeka, Croatia
Phone: +385 (51) 770 447

InTech China
Unit 405, Office Block, Hotel Equatorial Shanghai
No.65, Yan An Road (West), Shanghai, 200040, China
中国上海市延安西路65号上海国际贵都大饭店办公楼405单元
Phone: +86-21-62489820

Fax: +385 (51) 686 166
www.intechopen.com

Fax: +86-21-62489821

IntechOpen